Composite Structures 268 (2021) 114002

Contents lists available at ScienceDirect

Composite Structures

journal homepage: www.elsevier.com/locate/compstruct

A comprehensive micromechanical and experimental study of the electrical conductivity of polymeric composites incorporating carbon nanotube and carbon fiber

Taegeon Kil [a], D.W. Jin [a], Beomjoo Yang [b], H.K. Lee [a,*]

[a] Department of Civil and Environmental Engineering, Korea Advanced Institute of Science and Technology (KAI ST), 291 Daehak-ro, Yuseong-gu, Daejeon 34141, Republic of Korea
[b] School of Civil Engineering, Chungbuk National University, 1 Chungdae-ro, Seowon-gu, Cheongju, Chungbuk 28644, Republic of Korea

ARTICLE INFO

Keywords:
Polymer-matrix composites (PMCs)
Carbon nanotubes
Electrical properties
Micromechanics

ABSTRACT

The present study proposes a micromechanical model composed of a two-level homogenization process for predicting the electrical conductivity of polymeric composites incorporating carbon nanotube (CNT) and carbon fiber (CF). The curviness of the CNT and the interfacial resistivity between the polymer matrix and the CNT are considered in the micromechanical model. A series of numerical studies with model parameters are carried out, after which a genetic algorithm is applied to determine the optimized model parameters. The electrical and morphological properties of the composites are experimentally evaluated according to the content of CNT and CF. To verify the predictive capability of the proposed model, the present prediction is compared with that obtained from experiments. The proposed model combined with the genetic algorithm is found to closely simulate the effective electrical conductivity of the composites, as evidenced by the credible accuracy to the experimentally measured values.

1. Introduction

Conductive polymeric composites, which incorporate an electrically conductive filler in a polymer matrix, have been widely investigated as part of the effort to use these composites in strain-detecting sensors, supercapacitors, and electromagnetic interference shielding materials [1–6]. A conductive filler generally has the effect of improving the stiffness and strength together with the electrical conductivity [4,7,8]; therefore, considerable works have focused on conductive polymeric composites incorporating conductive fillers [9,10].

Carbon nanotube (CNT) can be considered as an attractive electrically conductive filler for the fabrication of conductive polymeric composites. CNT has a high aspect ratio and exceptional electrical conductivity as high as $1.7 - 2.0 \times 10^6$ S/m [11–13]. Therefore, conductive polymeric composites incorporating CNT as a type of conductive filler have been studied in an effort to realize enhanced engineering properties [10,14]. Zheng et al. [10] developed a polydimethylsiloxane composite sensor containing CNT and carbon black as fillers. The composite sensor showed high repeatability, stability, and reproducibility under different strains. Park et al. [15] deposited CNT onto the surface of carbon fiber (CF) to fabricate polyphenylene sulfide composites, reporting that introducing CNT onto the CF surface improved the interfacial, electrical, and flexural properties of fabricated composites.

Recently, a study of the use of a multiscale conductive filler composed of nano- and micro-scale materials was also reported [16,17]. Multiscale conductive fillers-incorporated composites show great differences with regard to the mechanisms embedded in the composites and in performance outcomes compared to conventional materials due to the vastly different scales and the inherent properties of the fillers [16,17]. This type of multiscale conductive filler-incorporated composites can offer synergetic effects through a combination of different fillers and can reduce the fabrication cost of composites by optimizing the filler content [10,16]. In this regard, a novel and elaborate model is required to gain a thorough understanding and to predict the characteristics of composites.

Hassanzadeh-Aghdam et al. [18] proposed a multiscale micromechanical model to predict the elastic properties of CNT/CF-reinforced polymeric composites. They used a micromechanical equation consisting of a simplified unit cell and Eshelby methods to describe the elastic modulus of the composites [18]. A micromechanical analysis based on the modified Mori-Tanaka method was con-

* Corresponding author.
E-mail address: haengki@kaist.ac.kr (H.K. Lee).

https://doi.org/10.1016/j.compstruct.2021.114002
Received 2 November 2020; Revised 2 April 2021; Accepted 13 April 2021
Available online 17 April 2021

ducted by Sung et al. [19] to address the thermal conductivity of CNT/woven fiber-incorporated epoxy composites. In their derivation, they initially adopted a modified form of the Mori-Tanaka method to predict the thermal conductivity of CNT-incorporated composites. A woven fabric composite model was adopted to estimate the effective thermal conductivity of CNT/woven fabric composites [19]. However, only a few studies have presented a theoretical method capable of predicting the effective electrical properties of multiscale conductive filler-incorporated composites. Moreover, in-depth studies on the effect of the inherent properties of CNT on the electrical characteristics of polymeric composites incorporating CNT and CF have yet to be conducted.

Against this backdrop, the present study proposes a multiscale micromechanical model composed of a two-level homogenization process for predicting the electrical characteristics of polymeric composites incorporating CNT and CF. This study suggests a micromechanical model considering the curviness of CNT and the interfacial resistivity between the polymer matrix (e.g., polypropylene) and the CNT. A series of numerical studies with model parameters optimized via a genetic algorithm are conducted. In addition, the electrical conductivity of the composites are experimentally measured and the microstructures of the composites are observed through scanning electron microscopy (SEM). To verify the applicability of the proposed model, the predicted electrical conductivity levels are compared with experimentally obtained values.

2. Micromechanical modeling

2.1. Micromechanics-based effective electrical conductivity of polymeric composites

Let us consider polymeric composites consisting of a polymer matrix, CNT, and CF. Fig. 1 shows a flow chart of the proposed micromechanical model for the prediction of the effective electrical conductivity of polymeric composites. It is assumed in the present model that CNT and CF are randomly oriented and distributed [23,24].

Firstly, let us consider two-phase composites consisting of a polymer matrix with electrical conductivity σ_m (matrix phase) and straight CNT with electrical conductivities $\widehat{\sigma}_i^{CNT}(i = 1 \text{ and } 3)$ (filler phase), referring to the electrical conductivities of CNT along the in-plane and normal directions, respectively. '^' correspondingly represents the thinly coated CNT surrounded by interfacial resistivity ρ [20–22], which is considered as one of the parameters in the present model.

At the first level of homogenization, the effective-medium model [22,23] is adopted to predict the electrical conductivity for CNT-incorporated composites. The electrical conductivity of polymeric composites with CNT σ^e can be estimated by Eqs. (1) and (2), respectively, with Eqs. (3) and (4), as reported in earlier works [22,23]:

$$\frac{3c_0(\sigma_m-\sigma^e)}{\sigma_m+2\sigma^e}+\frac{c_1}{3}\left[\frac{2(\widehat{\sigma_1}^{CNT}-\sigma^e)}{\sigma_e+S_{11}(\widehat{\sigma_1}^{CNT}-\sigma^e)}+\frac{(\widehat{\sigma_3}^{CNT}-\sigma^e)}{\sigma_e+S_{33}(\widehat{\sigma_3}^{CNT}-\sigma^e)}\right]=0 \quad (1)$$

and

$$\widehat{\sigma_i}^{CNT}=\frac{\sigma_i^{CNT}}{1+\rho\sigma_i^{CNT}S_{ii}(1/\alpha_{CNT}+2)/(D/2)} \quad (2)$$

with

$$S_{11}=S_{22}=\begin{cases}\frac{\alpha_{CNT}}{2\left(1-\alpha_{CNT}{}^2\right)^{\frac{3}{2}}}\left[\cos^{-1}\alpha_{CNT}-\alpha_{CNT}\left(1-\alpha_{CNT}{}^2\right)^{\frac{1}{2}}\right], \alpha_{CNT}<1\\ \frac{\alpha_{CNT}}{2(\alpha_{CNT}{}^2-1)^{\frac{3}{2}}}\left[\left(\alpha_{CNT}(\alpha_{CNT}{}^2-1)^{\frac{1}{2}}-\cosh^{-1}\alpha_{CNT}\right], \alpha_{CNT}>1\end{cases} \quad (3)$$

$$S_{33}=1-2S_{11}$$

and

$$\alpha_{CNT}=\frac{L}{D} \quad (4)$$

In these equations, c_0 and c_1 denote the volume fractions of the matrix and the CNT, respectively; σ_i^{CNT} (i = 1 and 3) correspondingly represents the electrical conductivities of the CNT along the in-plane and normal directions not considering the interfacial resistivity; and S_{11}, S_{22}, and S_{33} are the components of the Eshelby's tensor for a spheroidal inclusion [22]. Here, α_{CNT} signifies the aspect ratio of the CNT. L and D denote the length and diameter of the CNT, respectively [22]. Note that the effective CNT aspect ratio $\alpha_{CNT}{}'$ considering the curviness of CNT based on a random walk will be described in Section 2.2.

At the second level of homogenization, let us consider two-phase composites consisting of a CNT-incorporated composite matrix with electrical conductivity σ^e (matrix phase) and CF with electrical conductivity σ^{CF} (filler phase). The Mori-Tanaka model is adopted for the homogenization of CF in the CNT-incorporated polymeric composites [23,24].

Following the Mori-Tanaka model, the effective electrical conductivity of the composites incorporating CNT and CF, denoted by σ^{comp}, can be explicitly expressed by Eq. (5) with Eqs. (6) and (7), as reported in earlier works [23,24]:

$$\sigma^{comp}=\sigma^e+\frac{\sigma^e\phi_1 T}{1-\phi_1[1-(\sigma^e T)/(\sigma^{CF}-\sigma^e)]} \quad (5)$$

with

$$T=\frac{\sigma^{CF}-\sigma^e}{3}\left[\frac{2}{\sigma^e+(\sigma^{CF}-\sigma^e)S_{11}{}'}+\frac{1}{\sigma^e+(\sigma^{CF}-\sigma^e)S_{22}{}'}\right] \quad (6)$$

and

$$S_{11}{}'=S_{22}{}'=\begin{cases}\frac{\alpha_{CF}}{2\left(1-\alpha_{CF}{}^2\right)^{\frac{3}{2}}}\left[\cos^{-1}\alpha_{CF}-\alpha_{CF}\left(1-\alpha_{CF}{}^2\right)^{\frac{1}{2}}\right], \alpha_{CF}<1\\ \frac{\alpha_{CF}}{2(\alpha_{CF}{}^2-1)^{\frac{3}{2}}}\left[\left(\alpha_{CF}(\alpha_{CF}{}^2-1)^{\frac{1}{2}}-\cosh^{-1}\alpha_{CF}\right], \alpha_{CF}>1\end{cases} \quad (7)$$

$$S_{33}{}'=1-2S_{11}{}'$$

where ϕ_1 represents the volume fraction of the CF and $S_{11}{}'$, $S_{22}{}'$, and $S_{33}{}'$ are the components of the Eshelby's tensor for a spheroidal inclusion, with α_{CF} representing the aspect ratio of the CF inclusion [23,24].

2.2. Effective CNT aspect ratio considering the curviness of CNT based on the random walk model

Eq. (1) is derived based on the assumption of straight CNT; nevertheless, the CNT in the matrix is, in fact, curved due to both its high aspect ratio and the viscosity of the matrix [25,26]. Curviness of the CNT can affect the electrical conductivity of the composites. Accordingly, the random walk model [27,28] is adopted here to consider the curviness effect of the CNT in the matrix. The physical characteristics of polymers are suitably described by adopting the random walk model. This model supposes that a polymer chain consists of many segments having an identical length with a random direction, independent of the previous step [27,28]. The present model uses the random walk model to consider the curviness of CNT, assuming that CNT is perfectly dispersed in the matrix. It should, thus, be noted that the present model could not predict the aggregation of the CNT.

Schematics of the random walk model considering the curviness of the CNT are shown in Fig. 2. It is assumed in this study that the CNT consists of n segments with a length of l, as shown in Fig. 2(a). Thus, the length of the CNTL can be expressed as Eq. (8) [28]:

$$L=nl \quad (8)$$

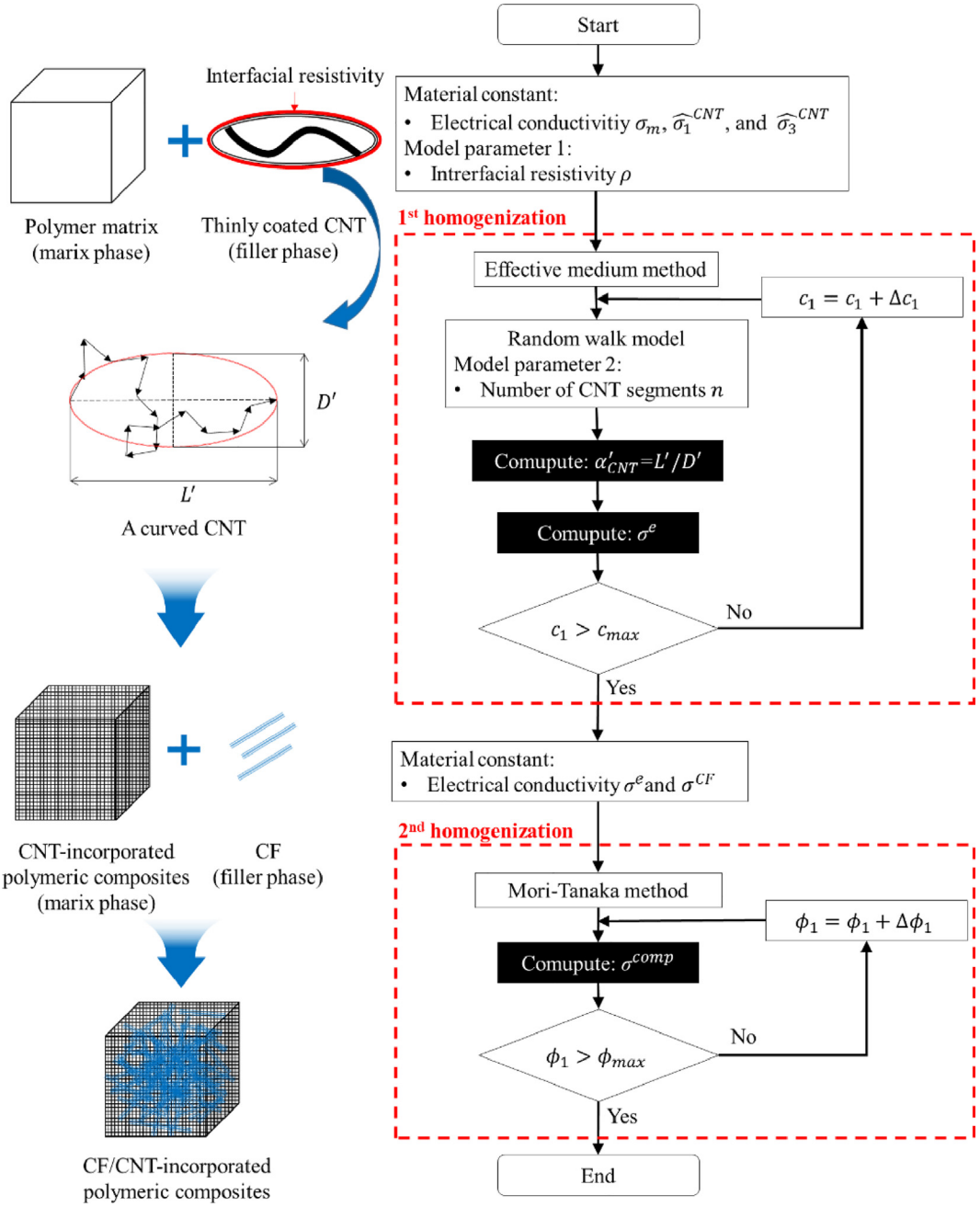

Fig. 1. Flow chart of the present micromechanical model for the prediction of the effective electrical conductivity of polymeric composites.

Based on the random walk model, the probability of finding the end of the CNT at the spherical shell can be approximated by a normal distribution function [28]. Accordingly, the effective length of the curved CNT $L^{'}$ can be estimated as Eq. (9) [27,28]:

$$L^{'} = \sqrt{< r^2 >_o} = \sqrt{n}l \tag{9}$$

where r is the radius of the spherical shell; <> indicates the average value; and the subscript o is used to represent the unperturbed state of the CNT, which has only short-range interaction as an ideal chain [27,28]. Consequently, the length of the CNT in Eq. (8) used to determine the aspect ratio of the CNT given in Eq. (4) is replaced by $L^{'}$ given in Eq. (9).

The effective diameter of the curved CNT $D^{'}$ can be determined as the twice radius of gyration R_g as shown in Fig. 2(b). R_g is defined as the average distances between the center of mass and each segment in the polymer chemistry field [27,28]. All CNT segments are projected from the end position P to the original position O [27,28], and the length of each projected segment l' on the x-z plane is assumed to be identical. R_g of the projected segments can therefore be expressed as Eq. (10) [27,28]:

$$R_g = \frac{1}{6}\sqrt{n}l' \tag{10}$$

To define the relationship between l' and l, fully stretched CNT in the x-direction is assumed, as shown in Fig. 2(c). The maximum length on the minor axis of the CNT ellipsoid d_{max} and the segment length with regard to the maximum length d_{unit} can be estimated geometrically. A one-dimensional random walk model is adopted here to calculate the expected value on the minor axis of the CNT ellipsoid d_{exp} from Eqs. (11) - (13), as reported in earlier works [29,30].

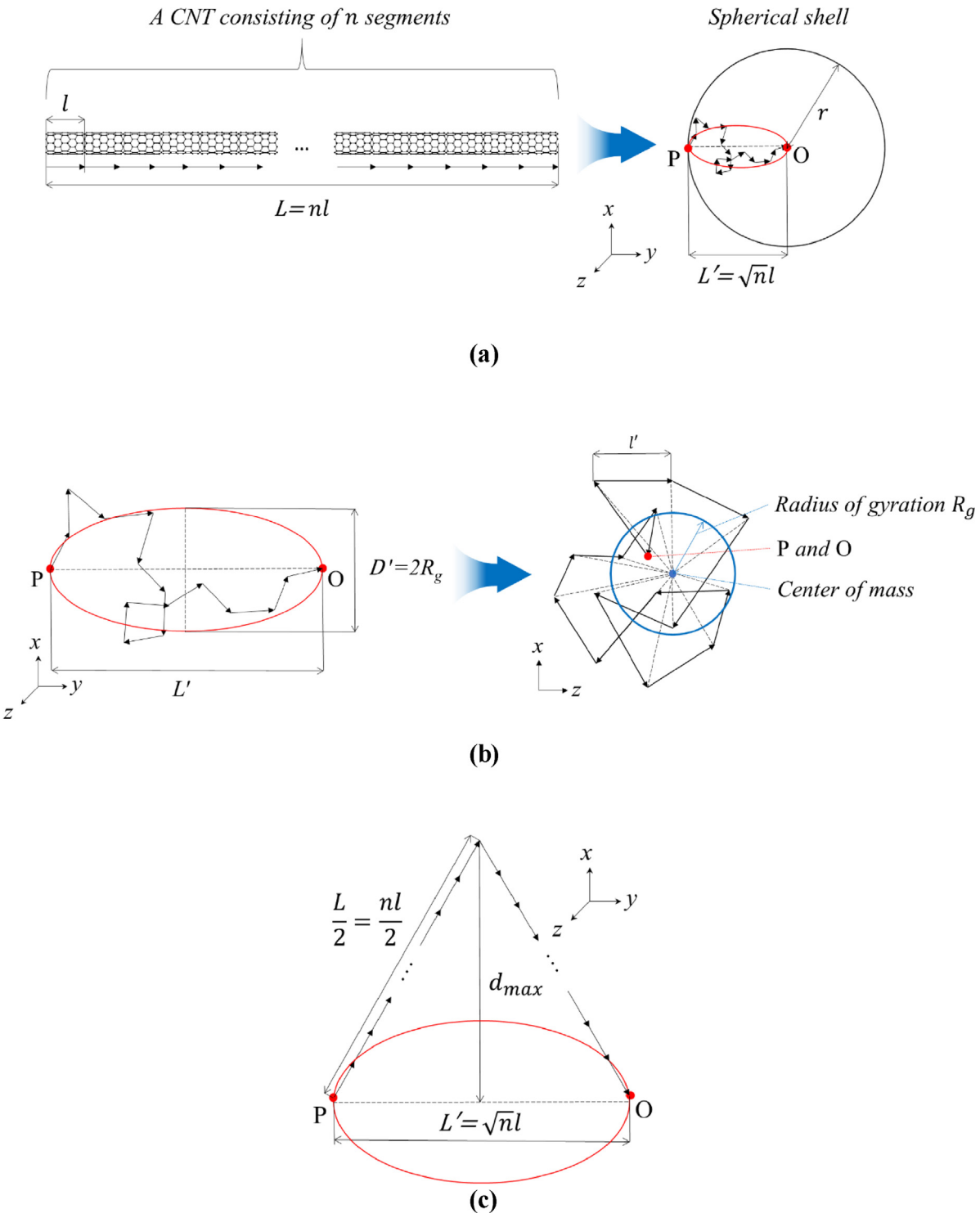

Fig. 2. Schematics of (a) a CNT consisting of n segments in accordance with the random walk model, (b) the effective diameter and length of a curved CNT and the radius of gyration of a CNT, and (c) a fully stretched CNT.

$$d_{max} = \frac{\sqrt{n^2 - n}}{2} l \tag{11}$$

$$d_{unit} = \frac{d_{max}}{n} = \frac{\sqrt{n^2 - n}}{2n} l \tag{12}$$

$$d_{exp} = \sqrt{\frac{2n}{\pi}} d_{unit} = \sqrt{\frac{n-1}{2\pi}} l \tag{13}$$

D' can be determined by assuming l' and l are proportional to d_{exp} and $L/2$, respectively, as expressed in Eq. (14).

$$D' = 2R_g = \frac{1}{3}\sqrt{\frac{2}{\pi}}\sqrt{\frac{n-1}{n}} l, (n > 1) \tag{14}$$

From Eqs. (9) - (14), the new aspect ratio of the CNT $\alpha_{CNT}{}'$ can be expressed by n, as expressed in Eq. (12).

$$\alpha_{CNT}{}' = \frac{L'}{D'} = \sqrt{\frac{\pi}{2}}\frac{3n}{\sqrt{n-1}}, (n > 1) \quad (15)$$

2.3. A genetic algorithm adopted for determining the model parameters

A genetic algorithm based on evolutionary computations is adopted to find the optimal values of the model parameters n and ρ in Eqs. (15) and (2), respectively. The genetic algorithm is one of the most effective approaches to converge to an optimal solution [31,32,44]. The basic steps of the genetic algorithm can be summarized as follows: 1) an artificial population, which consists of solution candidates, is randomly generated, 2) each solution candidate in the population is referred to as a chromosome, 3) each chromosome is evaluated by the selection operator and chromosomes with low fitness values is receded, 4) selection, crossover, and mutation are then applied to the best chromosome of the population and a new generation is created, and 5) at the end of the process, the chromosome with the highest fitness value is considered as an optimum solution [33,44].

A flow chart of the genetic algorithm for determining model parameters is shown in Fig. 3 (cf. [34, 35]). The parameters n and ρ are defined as the chromosome in the present study. The initial values of all parameters are assumed to be 0, and the ranges of the parameters were assumed as follows: $n = 1.0 - 1.0E6$ and $\rho = 0 - 1.0E\text{-}6$ S/m based on numerical studies. After the population of chromosomes is generated randomly, each chromosome is assessed in terms of the objective function F by Eq. (16), as follows [31,33,36],

$$F = \sum_{i=1}^{N} \left(\sigma^i - \sigma^{e(i)}\right)^2 \quad (16)$$

where N is the number of CNT-incorporated polypropylene composites with a different CNT content level, σ^i is the measured electrical conductivity of the i^{th} composites, and $\sigma^{e(i)}$ is the predicted electrical conductivity of the i^{th} composites given in Eq. (1) [36].

All measured electrical conductivities of the composites are input into Eq. (16), and the predicted electrical conductivity is calculated by micromechanics. The F values of all chromosomes are calculated automatically [35]. Selection, crossover, and mutation are applied to reproduce a new generation once the best chromosome with the lowest F is selected by selection operator [34]. This procedure is looped until the generation reaches 20000. The optimal n and ρ with the minimum F in all generations are updated.

3. Experimental program

Multi-walled CNT (Hyosung Inc.) produced by means of thermal chemical vapor deposition [37] with a purity level exceeding 95.0% was used in this study. The length of the CNT was approximately 10 μm and the diameter ranged from 12 to 40 nm. The electrical conductivity of the CNT in the normal direction was 1.9E4 S/m and the density of the CNT was 2.2 g/cm^3. CF (TORAYCA-T700S) supplied by ACE C & Tech. Co., Ltd. was used, and the length and diameter of the CF were 3.0 mm and 7.0 μm, respectively. The electrical resistivity and density of the CF were 1.6E-3 Ω · cm and 1.8 g/cm^3, respectively. Isotactic polypropylene (Sigma-Aldrich Inc.) was used as a polymer matrix. The approximate average molecular number and weight of the polypropylene were 67000 and 250000, respectively. A xylene solution (Samchun Inc.) was used as a solvent in order to melt the polypropylene homogeneously. Silica fume (Elkem Inc.) and a polycarboxylate-based superplasticizer (Dongnam Co., Ltd.) were added to disperse the CNT mechanically [38]. The properties of the silica fume and superplasticizer used here can be found from Kim et al. [38].

In total, ten composites were fabricated, as shown in Table 1. The CNT content of the CNT-incorporated polypropylene composites was varied from 0.5 to 5.0 wt% and the CF/CNT-incorporated composites were fabricated by varying the CF contents from 1.0 to 4.0 wt%. Note that the CNT content was fixed at 0.5 wt% for the composites incorporating CF and CNT.

A schematic description of the fabrication procedure and the photograph of electrical conductivity measurements of the composites are shown in Fig. 4. The CNT and dispersion agents (i.e., silica fume and a superplasticizer) were put into a beaker with 100 mL of xylene and the solution was sonicated for 1 h using tip-type ultrasonication equipment (Sonic & Materials, USA), where the pulse on/off was 10 sec and the amplitude was 17.5 μm [39]. Subsequently, 15 g of the polypropylene and 300 mL of the xylene were stirred on a hotplate for 1 h at 260 °C until the polypropylene was completely melted [40]. The CNT-dispersed solution, the melted polypropylene, and the CF were mixed together while the mixture was heated for about 3 h, until all of the xylene evaporated. Note that the CF was not incorporated in the CNT-incorporated polypropylene composites. The fabricated composite solids were dried at 70 °C for 24 h until complete solidification. Finally, the dried composite solids were cut into parti-

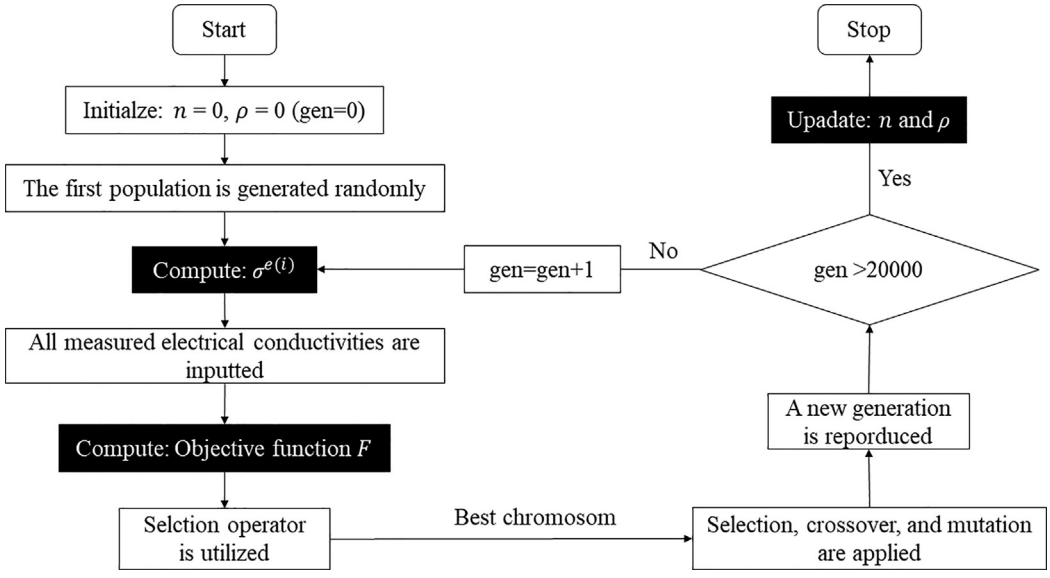

Fig. 3. Flow chart of the genetic algorithm for determining model parameters (cf. [34,35]).

Table 1
Mix proportions of the CF/CNT-incorporated polypropylene composites expressed in terms of the mass ratio (wt%).

Composites	Polypropylene	CNT	CF	Silica fume	Superplasticizer
CNT_0.5	100	0.5	–	5	3.2
CNT_1.0	100	1.0	–	5	3.2
CNT_2.0	100	2.0	–	5	3.2
CNT_3.0	100	3.0	–	5	3.2
CNT_4.0	100	4.0	–	5	3.2
CNT_5.0	100	5.0	–	5	3.2
CF_1.0/CNT_0.5*	100	0.5	1.0	5	3.2
CF_2.0/CNT_0.5	100	0.5	2.0	5	3.2
CF_3.0/CNT_0.5	100	0.5	3.0	5	3.2
CF_4.0/CNT_0.5	100	0.5	4.0	5	3.2

* CF/CNT-incorporated polypropylene composites with 0.5 wt% CNT, 1.0 wt% CF, 5.0 wt% silica fume, and 3.2 wt% superplasticizer.

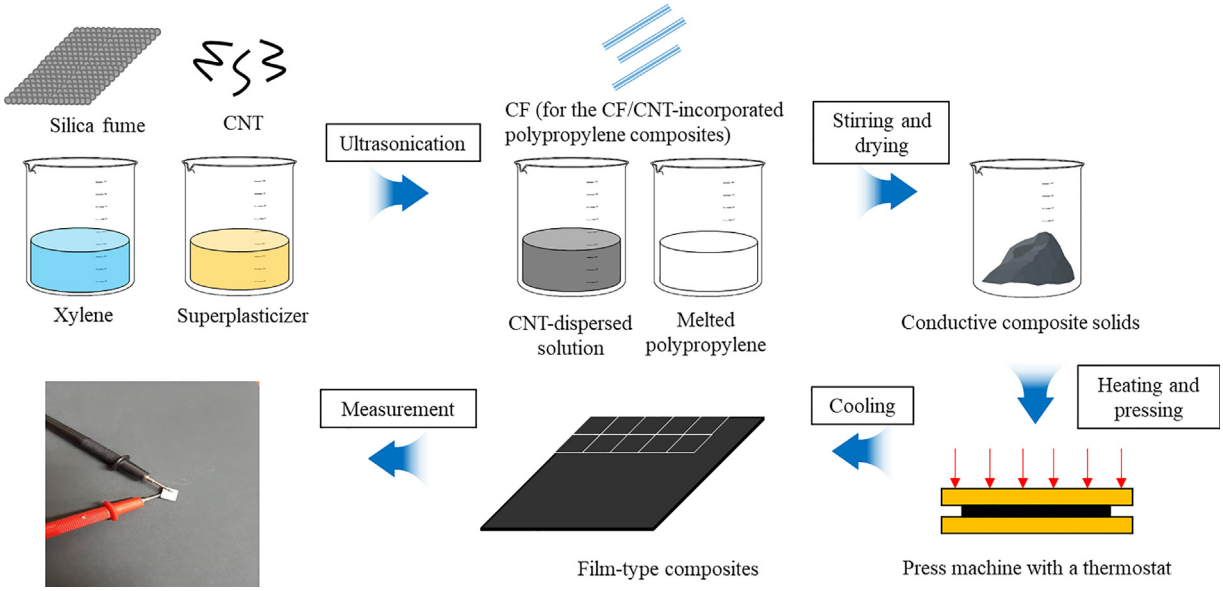

Fig. 4. Schematic description of the fabrication procedure and the photograph of electrical conductivity measurements of the composites.

cles with a radius of around 50 mm and were put on a mold with dimensions of 100 mm × 100 mm × 0.5 mm in a press machine with a thermostat. The temperature and pressure were increased to 220 ˚C and 40 MPa, respectively, for 5 min. The film-type composites were then cooled to room temperature.

Both sides of the composites were covered with silver paste as electrodes, after which they were cut into ten composites each 10 mm × 10 mm × 0.5 mm in size. The electrical resistance of the composites was measured by the two-probe method with a digital multimeter (Keysight Technologies U1281A) [41]. The average value of the electrical resistance levels of ten replicas served as the representative resistance, which was then converted into the electrical conductivity using the Eq. (17) [41]:

$$\sigma = \frac{L}{RA} \tag{17}$$

where σ is the electrical conductivity (S/m), R is the electrical resistance (Ω), A is the cross-sectional area (cm^2), and L is the distance between the sides of the composites (cm) [41].

SEM and optical microscopy were used to observe the morphological characteristics of the composites. For the SEM image analysis, composites were coated with Pt using an ion beam sputter-coating device under a low vacuum (Hitachi Co. FE-SEM SU5000). For the optical microscopy image analysis, the same composites as used for the SEM image analysis were observed with a resolution of 2592 × 1944 at 2300 magnifications (HiMaxTech Co. HT1004).

4. Results and discussion

4.1. Numerical simulation

Based on the present proposed model, a series of numerical studies are conducted to elucidate the correlations between the model parameters and the electrical conductivity of the composites. In this simulation, it is assumed for the composites that the following material properties are applied: $L = 10$ μm, $\sigma_m = 1.0E\text{-}12$ S/m, and ${\sigma_3}^{CNT} = 1.9E7$ S/m. ${\sigma_1}^{CNT}$ is expressed as ${\sigma_1}^{CNT} = {\sigma_3}^{CNT}/1000$ [22,25].

The new aspect ratio of CNT $\alpha_{CNT}{}'$ against the number of CNT segments n is simulated as shown in Fig. 5(a). $\alpha_{CNT}{}'$ decreases as n decreases. That is, a lower value of n leads to a lower aspect ratio of the CNT. The predicted electrical conductivity of the CNT-incorporated polypropylene composites σ^e against the CNT content while varying n is depicted in Fig. 5(b). n has a significant effect on both σ^e and the percolation threshold of the composites. A higher value of n results in an earlier percolation threshold response. These results indicate that using CNT with a higher n leads to a more rapid percolation threshold due to the higher aspect ratio of the CNT. These simulation results are in agreement with earlier predictions [16,17] which suggest that $\alpha_{CNT}{}'$ has a significant effect on σ^e and the percolation threshold.

An additional numerical study is carried out to analyze the electrical properties of the CNT-incorporated polymeric composites, reflect-

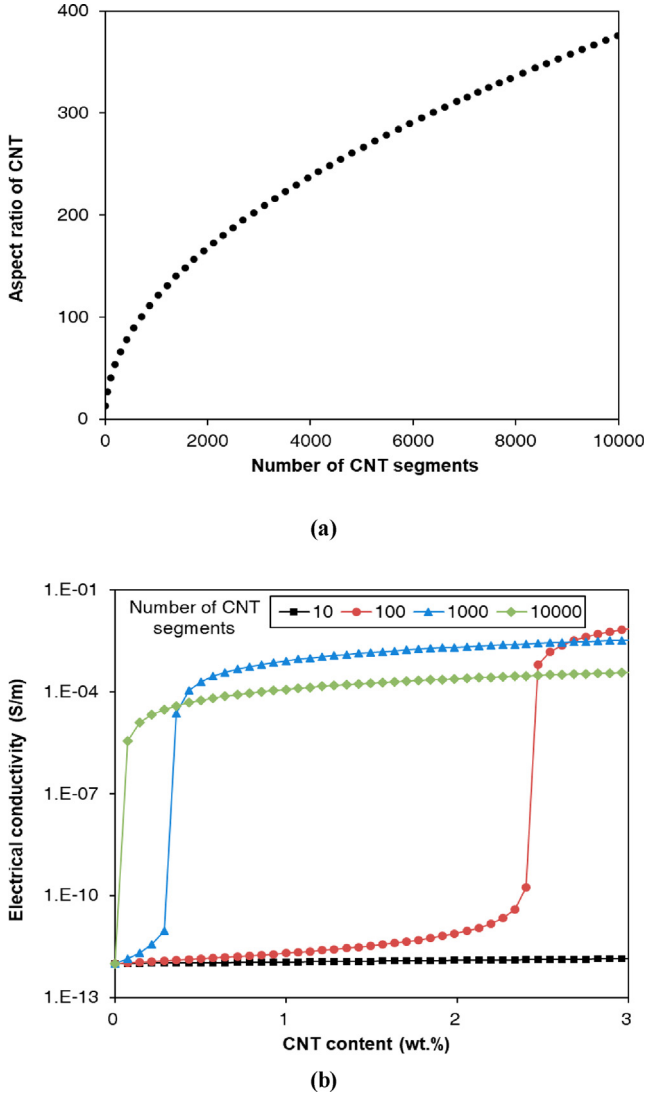

Fig. 5. (a) New aspect ratio of CNT against the number of CNT segments and (b) the predicted electrical conductivity of CNT-incorporated polypropylene composites against the CNT content while varying the number of CNT segments.

ing the interfacial resistivity ρ between the polypropylene matrix and the CNT. Here, n is assumed to be 1000. The predicted electrical conductivity of the composites against the CNT content while varying the interfacial resistivity is shown in Figs. 6. In this case, ρ has a weaker effect on the percolation threshold. Meanwhile, σ^e decreases noticeably past the percolation threshold as ρ increases from 1.0E-10 to 1.0E-7 m^2/S. Therefore, the results in Fig. 6 show that ρ plays an important role in how it affects σ^e past the percolation threshold.

Lastly, the predicted electrical conductivity of the CF/CNT-incorporated polypropylene composites σ^{comp} against the CF content while varying the CNT content and CF length are shown in Fig. 7. The material properties of the CF adopted here are identical to those in the present experimental study (see Section 3). The model parameters of the CNT are assumed to be n = 1000 and ρ = 1.0E-9 m^2/S within the range of the model parameters in Figs. 5(b) and (6). Fig. 7(a) shows that initial electrical conductivity of the composites at the CF content of 0.0 wt% increases considerably given that the CNT was incorporated during the first level of homogenization. In the 0.5 wt% CNT case, σ^{comp} increases remarkably as the CF content increases. The outcomes of σ^{comp} against the CF content while varying

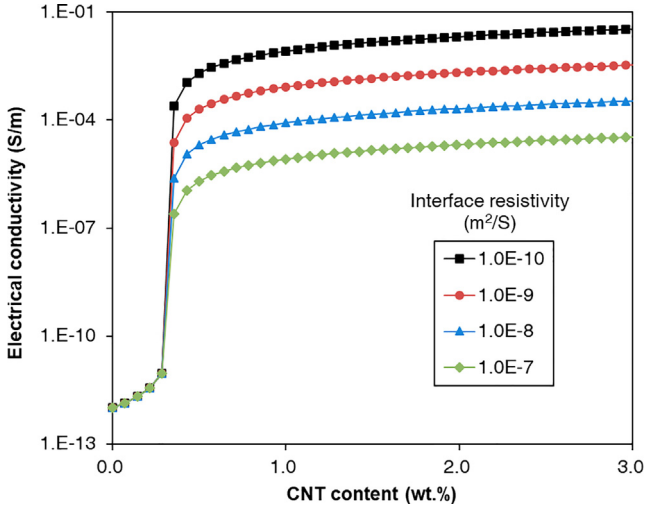

Fig. 6. Predicted electrical conductivity of CNT-incorporated polypropylene composites against the CNT content while varying the interfacial resistivity.

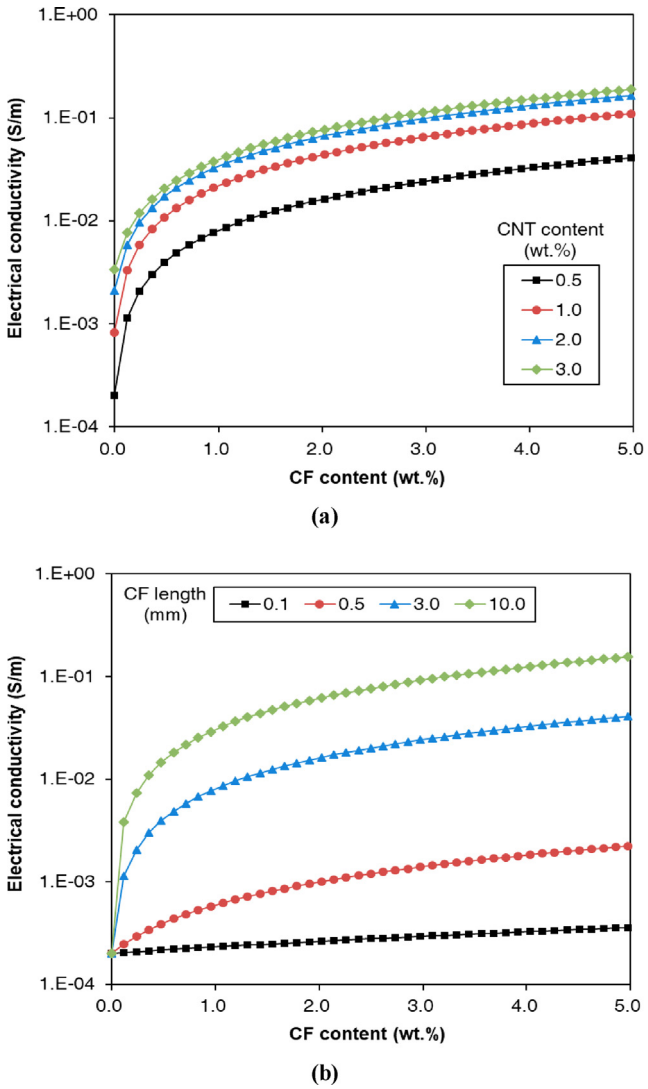

Fig. 7. Predicted electrical conductivity of CF/CNT-incorporated polypropylene composites against the CF content while varying (a) the CNT content and (b) the CF length.

the CF length are shown in Fig. 7(b). Here, the CNT content is fixed at 0.5 wt%. It can be observed that the incorporation of CF leads to an increase in σ^{comp} [42]. In particular, σ^{comp} increases drastically until the CF content reaches 1.0 wt%, and this effect becomes more pronounced as the CF length increases. This result indicates that a higher value of α_{CF} leads to an increase in σ^{comp}. The result shown in Fig. 7(b) is in good agreement with the prediction made by Pal et al. [17], who found that a high α_{CF} helps to improve σ^{comp} even at low CF content levels.

4.2. Experimental results

The measured electrical conductivity of the CF/CNT-incorporated polypropylene composites are listed in Table 2. The electrical conductivity of the CNT-incorporated polypropylene composites increased sharply from 1.0E-12 to 4.2E-3 S/m with 0.5 wt% CNT incorporated into them; the percolation threshold of the composites should arise when the CNT content is lower than 0.5 wt%. Past the percolation threshold, the electrical conductivity of the CNT-incorporated polypropylene composites increased continually to 4.1E-1 S/m when 5.0 wt% CNT was incorporated. These results indicate that the electrical conductivity of the composites increases as the CNT content is increased, leading to the formation of an electrically conductive network due to the increased contact between adjacent CNTs [41]. The electrical conductivity of the CF/CNT-incorporated polypropylene composites surpassed that of the CNT_0.5 composites and improved as the CF content was increased. This improvement can be explained by the bridging effect of the CNT, by which the presence of the CNT can connect the independently separated CF and form a 3-D hierarchical network structure in the composites [16].

SEM images of the CNT_0.5 composites and the CF_4.0/CNT_0.5 composites are shown in Fig. 8. The SEM images in Fig. 8(a) depict the morphology and structure of the CNT_0.5 composites. CNT is shown to be dispersed clearly as an individual filler material with the silica fume, having a random distribution. It was also observed that the thickness of each individual CNT was in the range of 40 – 50 nm with an electrically conductive network also having formed. The CNT is curved significantly in the polypropylene matrix, and this phenomenon affects the CNT aspect ratio. Fig. 8(b) shows the morphology of the CF_4.0/CNT_0.5 composites; here, CF and CNT are found together on the fracture surfaces of the composites. This is evidence that the electrical conductivity of the composites can be improved via the bridging effect between the CF and CNT [43]. The CNT was curved, while the CF maintained its original shape in the polypropylene matrix. Fig. 8(c) shows the optical microscopy image of the CF_4.0/CNT_0.5 composites. As assumed in the present model, the CF was found to be randomly distributed.

Table 2
Measured electrical conductivity the CF/CNT-incorporated polypropylene composites.

Composites	Electrical conductivity (S/m)
CNT_0.0	1.0E-12
CNT_0.5	4.2E-3
CNT_1.0	7.4E-2
CNT_2.0	1.2E-1
CNT_3.0	1.7E-1
CNT_4.0	2.8E-1
CNT_5.0	4.1E-1
CF_1.0/CNT_0.5	2.8E-2
CF_2.0/CNT_0.5	3.6E-2
CF_3.0/CNT_0.5	4.1E-2
CF_4.0/CNT_0.5	8.1E-2

4.3. Comparisons between the present prediction and experimental results

Comparisons of the effective electrical conductivity of the composites between the present prediction and experimental results are made. The methods adopted and material parameters are identical to those used in Sections 3 and 4.1. The model parameters n and ρ are determined using a genetic algorithm, as explained in Section 2.3. Fig. 9 (a) shows the normalized root mean square error of the objective function F corresponding to different population sizes. This result indicates that the normalized root mean square error decreases as the population size increases [36]. The best value of F against generation while varying the population sizes is shown in Fig. 9(b). The best value represents the minimum result of the objective function within the current generation [36]. Both best values of F at population sizes of 100 and 200 decrease significantly as the number of generations increases, converging to 0.27 at 20000. The other values at population sizes of 10, 30, and 50 converge to 3.76 at 20000. Hence, the population size in the present model is determined to be 100 based on the test results, and the model parameters estimated by the genetic algorithm are $n = 751$ and $\rho = 2.1\text{E-}11\ \text{m}^2/\text{S}$.

The electrical conductivity of CNT-incorporated polypropylene composites, which was predicted with the optimized parameters through curve-fit to the present experimental result, is shown in Fig. 10(a). Overall, the present prediction is in good agreement with the experimental result as tabulated in Table 2. The percolation threshold in the present prediction is formed at 0.44 wt% CNT [22,23], similar to that obtained in the experiment with less than 0.5 wt% CNT. This comparison indicates that the proposed model combined with the genetic algorithm closely simulates the electrical conductivity of the composites. Fig. 10(b) shows the comparison of the effective electrical conductivity of CF/CNT-incorporated polypropylene composites σ^{comp} between the present prediction with the fitted parameters and the present experimental result. σ^{comp} improves in both the simulation and the experimental result with an increase in the CF content. From this comparison, our modeling results provide higher values of σ^{comp} as compared to the experimental result. The assumption that the electrically conductive fillers are homogenized completely in the matrix can be attributable to the differences between the simulation and the experimental result.

5. Concluding remarks

A comprehensive micromechanical and experimental study of the electrical conductivity of polymeric composites incorporating CNT and CF was conducted. A two-level homogenization process based on micromechanics was used to predict the effective electrical conductivity of the composites. The CNT curviness and interfacial resistivity between the matrix and CNT were considered. Numerical studies with model parameters were carried out, after which the model parameters were estimated using a genetic algorithm. In addition, the study measured the electrical conductivities and observed the morphological characteristics of polymeric composites. Comparisons of the effective electrical conductivity of the composites between the present prediction and the experimental result were also conducted.

In numerical studies of the proposed model, a higher number of CNT segments was found to lead to an earlier percolation threshold, while the interfacial resistivity was mainly shown to affect the effective electrical conductivity past the percolation threshold. The CF length also played an important role in the effective electrical conductivity of the composites. The measured electrical conductivity of the CNT-incorporated polypropylene composites indicated that the percolation threshold arises with less than 0.5 wt% of CNT content, while the measured electrical conductivity of the CF/CNT-incorporated polypropylene composites improves as the CF content increases. Comparisons of the present prediction and experimental results of the

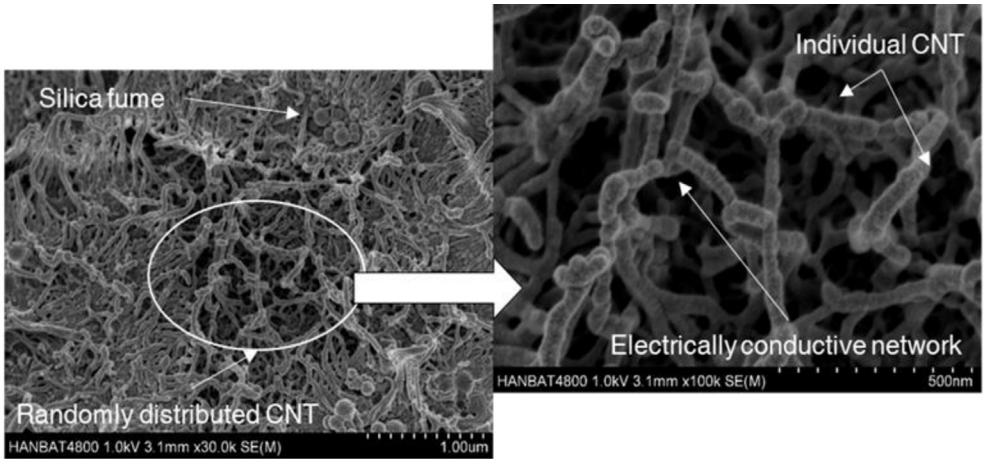

(a)

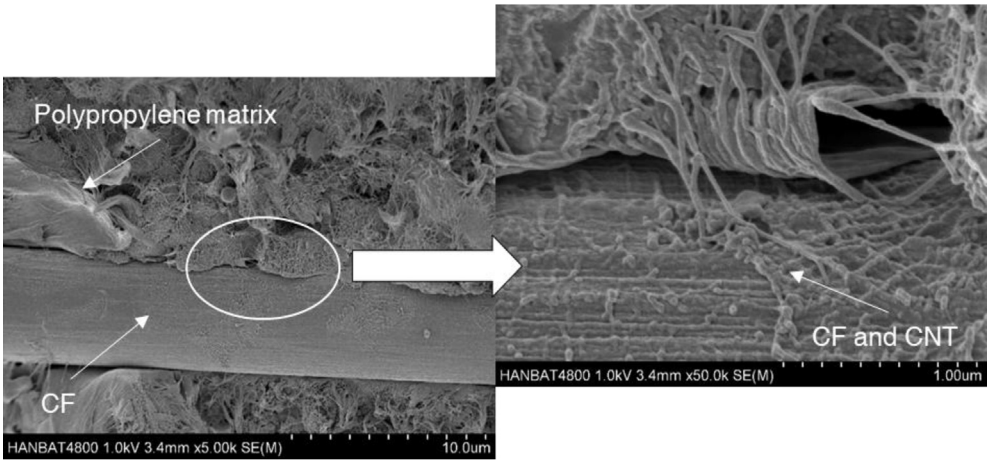

(b)

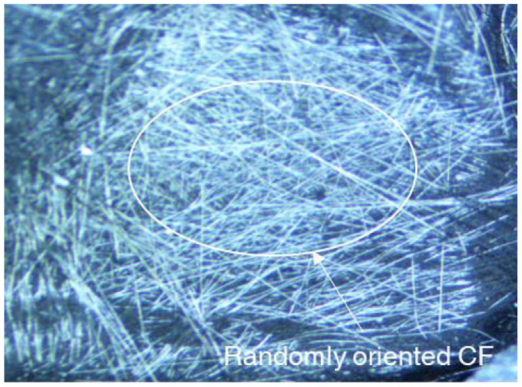

(c)

Fig. 8. SEM images of (a) the CNT_0.5 composites and (b) the CF_4.0/CNT_0.5 composites and (c) optical microscopy image of the CF_4.0/CNT_0.5 composites.

effective electrical conductivity of the composites found that the prediction is in good agreement with the experimentally measured value. The percolation threshold in the present prediction was found to arise at 0.44 wt% CNT, and the effective electrical conductivity of the composites improved in both the simulation and experimental result with an increase in the electrically conductive filler content.

This study demonstrates the applicability of a micromechanical model consisting of a two-level homogenization process to predict the effective electrical conductivity of multiscale conductive filler-incorporated composites. However, to examine the applicability of the present scheme, additional theoretical and experimental verifications incorporating various electrically conductive fillers (i.e., gra-

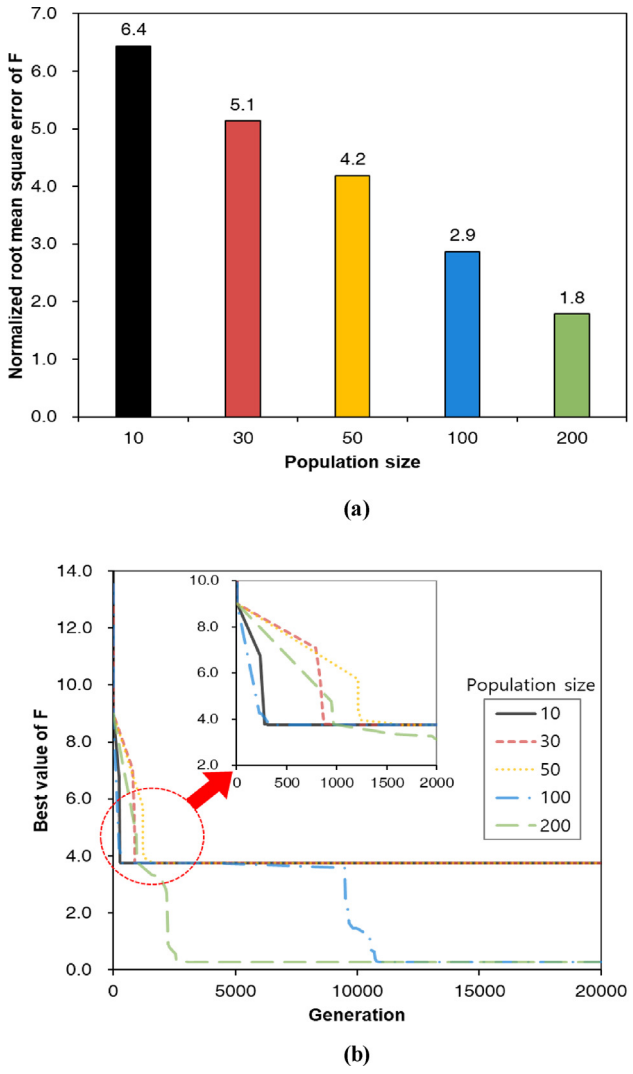

Fig. 9. (a) The normalized root mean square error of the objective function *F* corresponding to different population sizes and (b) the best value of *F* against generation while varying the population size.

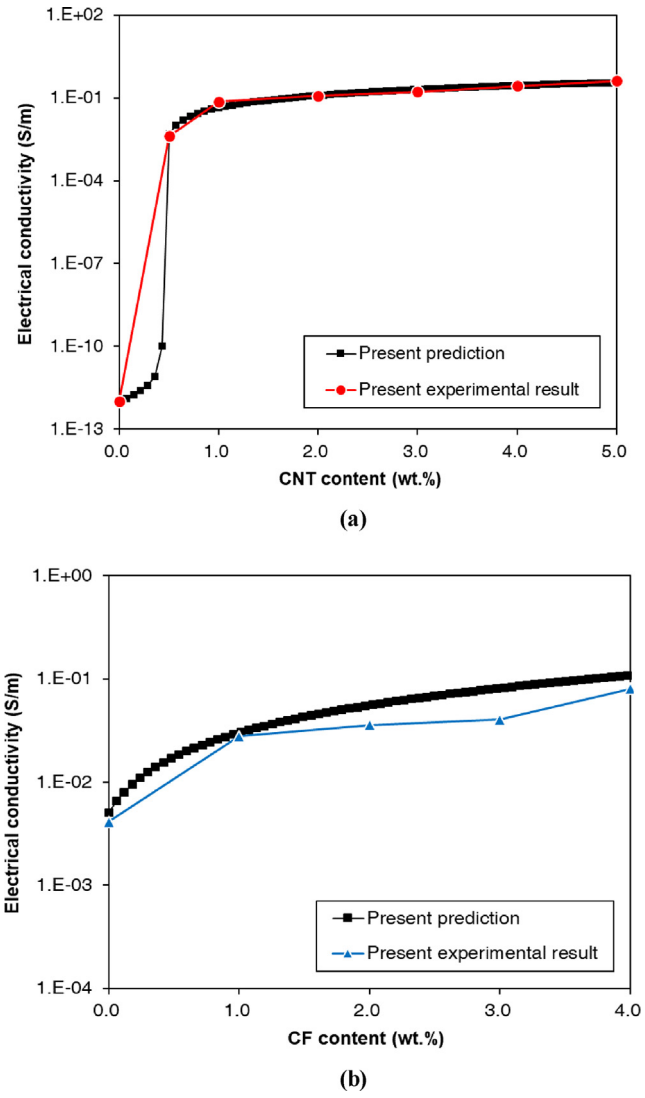

Fig. 10. (a) The electrical conductivity of CNT-incorporated polypropylene composites, which was predicted with the optimized parameters through curve-fit to the present experimental result; (b) the comparison of the effective electrical conductivity of CF/CNT-incorporated polypropylene composites between the present prediction with the fitted parameters and the present experimental result.

phene, carbon black, and carbon nanofiber etc.) must be carried out. In addition, the effect of electron tunneling between electrically conductive fillers was not considered in the present study. The electron tunneling effect could affect the effective electrical conductivity of polymeric composites. Accordingly, our future work will examine the effects of electrical tunneling on the electrical conductivity of these types of composites.

CRediT authorship contribution statement

Taegeon Kil: Conceptualization, Software, Data curation, Resources, Writing - original draft. **D.W. Jin:** Investigation, Methodology, Formal analysis. **Beomjoo Yang:** Visualization, Validation, Writing - review & editing. **H.K. Lee:** Supervision, Project administration.

Declaration of Competing Interest

The authors declare that they have no known competing financial interests or personal relationships that could have appeared to influence the work reported in this paper.

Acknowledgments

This research was supported by a grant from the National Research Foundation of Korea (NRF) funded by the Korean government (No.2018R1A2A1A05076894). Mr. J.H. Seo at KAIST for writing assistance.

References

[1] Roh E, Hwang BU, Kim D, Kim BY, Lee NE. Stretchable, transparent, ultrasensitive, and patchable strain sensor for human–machine interfaces comprising a nanohybrid of carbon nanotubes and conductive elastomers. ACS Nano 2015;9(6):6252–61.

[2] Zhang K, Li GH, Feng LM, Wang N, Guo J, Sun K, et al. Ultralow percolation threshold and enhanced electromagnetic interference shielding in poly (L-lactide)/multi-walled carbon nanotube nanocomposites with electrically conductive segregated networks. J Mater Chem C 2017;5(36):9359–69.

[3] Lin L, Liu S, Zhang Q, Li X, Ji M, Deng H, et al. Towards tunable sensitivity of electrical property to strain for conductive polymer composites based on thermoplastic elastomer. ACS Appl Mater Interfaces 2013;5(12):5815–24.

[4] Liu H, Gao J, Huang W, Dai K, Zheng G, Liu C, et al. Electrically conductive strain sensing polyurethane nanocomposites with synergistic carbon nanotubes and graphene bifillers. Nanoscale 2016;8(26):12977–89.
[5] Wang K, Zhao P, Zhou X, Wu H, Wei Z. Flexible supercapacitors based on cloth-supported electrodes of conducting polymer nanowire array/SWCNT composites. J Mater Chem 2011;21(41):16373–8.
[6] Wen M, Sun X, Su L, Shen J, Li J, Guo S. The electrical conductivity of carbon nanotube/carbon black/polypropylene composites prepared through multistage stretching extrusion. Polymer 2012;53(7):1602–10.
[7] Song Q, Ye F, Yin X, Li W, Li H, Liu Y, et al. Carbon nanotube–multilayered graphene edge plane core–shell hybrid foams for ultrahigh-performance electromagnetic-interference shielding. Adv Mater 2017;29(31):1701583.
[8] He D, Fan B, Zhao H, Lu X, Yang M, Liu Y, et al. Design of electrically conductive structural composites by modulating aligned CVD-grown carbon nanotube length on glass fibers. ACS Appl Mater Interfaces 2017;9(3):2948–58.
[9] Yang BJ, Jang JU, Eem SH, Kim SY. A probabilistic micromechanical modeling for electrical properties of nanocomposites with multi-walled carbon nanotube morphology. Compos Part A-Appl S 2017;92:108–17.
[10] Zheng Y, Li Y, Dai K, Wang Y, Zheng G, Liu C, et al. A highly stretchable and stable strain sensor based on hybrid carbon nanofillers/polydimethylsiloxane conductive composites for large human motions monitoring. Compos Sci Technol 2018;156:276–86.
[11] Dang ZM, Zheng MS, Zha JW. 1D/2D carbon nanomaterial-polymer dielectric composites with high permittivity for power energy storage applications. Small 2016;12(13):1688–701.
[12] Chu K, Park SH. Electrical heating behavior of flexible carbon nanotube composites with different aspect ratios. J Ind Eng Chem 2016;35:195–8.
[13] Ebbesen TW, Lezec HJ, Hiura H, Bennett JW, Ghaemi HF, Thio T. Electrical conductivity of individual carbon nanotubes. Nature 1996;382(6586):54–6.
[14] Wu HY, Jia LC, Yan DX, Gao JF, Zhang XP, Ren PG, et al. Simultaneously improved electromagnetic interference shielding and mechanical performance of segregated carbon nanotube/polypropylene composite via solid phase molding. Compos Sci Technol 2018;156:87–94.
[15] Park M, Park JH, Yang B, Cho J, Kim SY, Jung I. Enhanced interfacial, electrical, and flexural properties of polyphenylene sulfide composites filled with carbon fibers modified by electrophoretic surface deposition of multi-walled carbon nanotubes. Compos Part A-Appl S 2018;109:124–30.
[16] Kim GM, Yang BJ, Yoon HN, Lee HK. Synergistic effects of carbon nanotubes and carbon fibers on heat generation and electrical characteristics of cementitious composites. Carbon 2018;134:283–92.
[17] Pal G, Kumar S. Multiscale modeling of effective electrical conductivity of short carbon fiber-carbon nanotube-polymer matrix hybrid composites. Mater Des 2016;89:129–36.
[18] Hassanzadeh-Aghdam MK, Ansari R, Darvizeh A. Micromechanical analysis of carbon nanotube-coated fiber-reinforced hybrid composites. Int J Eng Sci 2018;130:215–29.
[19] Sung DH, Kim M, Park YB. Prediction of thermal conductivities of carbon-containing fiber-reinforced and multiscale hybrid composites. Compos. Part B-Eng 2018;133:232–9.
[20] Nan CW, Birringer R, Clarke DR, Gleiter H. Effective thermal conductivity of particulate composites with interfacial thermal resistance. J Appl Phys 1997;81 (10):6692–9.
[21] Duan HL, Karihaloo BL. Effective thermal conductivities of heterogeneous media containing multiple imperfectly bonded inclusions. Phys Rev B 2007;75 (6):064206.
[22] Wang Y, Weng GJ, Meguid SA, Hamouda AM. A continuum model with a percolation threshold and tunneling-assisted interfacial conductivity for carbon nanotube-based nanocomposites. J Appl Phys 2014;115(19):193706.
[23] Xia X, Hao J, Wang Y, Zhong Z, Weng GJ. Theory of electrical conductivity and dielectric permittivity of highly aligned graphene-based nanocomposites. J Phs Condes Matter 2017;29:205702.
[24] Weng GJ. A dynamical theory for the Mori-Tanaka and Ponte Castañeda-Willis estimates. Mech Mater 2010;42(9):886–93.
[25] Kim GM, Yang BJ, Cho KJ, Kim EM, Lee HK. Influences of CNT dispersion and pore characteristics on the electrical performance of cementitious composites. Compos Struct 2017;164:32–42.
[26] Yang BJ, Cho KJ, Kim GM, Lee HK. Effect of CNT agglomeration on the electrical conductivity and percolation threshold of nanocomposites: a micromechanics-based approach. CMES-Comput Model Eng Sci 2014;103(5):343–65.
[27] Bower DI. An introduction to polymer physics, 2003.
[28] Rubin RJ. Random-Walk Model of Chain-Polymer Adsorption at a Surface. J Chem Phys 1965;43(7):2392–407.
[29] Hughes BD. Random walks and random environments. 2. Random environments. Clarendon Press 1996.
[30] Kehr K, Kutner R. Random walk on a random walk. Phy Sica A 1982;110 (3):535–49.
[31] Bäck T, Fogel DB, Michalewicz Z. Handbook of evolutionary computation. CRC Press; 1997.
[32] Fraser AS. Simulation of genetic systems by automatic digital computers vi. epistasis. Aust. J Biol Sci 1960;13(2):150–62.
[33] Saka MP, Hasançebi O, Geem ZW. Metaheuristics in structural optimization and discussions on harmony search algorithm. Swarm Evol Comput 2016;28:88–97.
[34] Kanagarajan D, Karthikeyan R, Palanikumar K, Davim JP. Optimization of electrical discharge machining characteristics of WC/Co composites using non-dominated sorting genetic algorithm (NSGA-II). The Int J Adv Manuf Tech 2008;36(11–12):1124–32.
[35] Mathias JD, Balandraud X, Grediac M. Applying a genetic algorithm to the optimization of composite patches. Comput struct 2006;84(12):823–34.
[36] Jeon H, Yu J, Lee H, Kim G, Kim JW, Jung YC, et al. A combined analytical formulation and genetic algorithm to analyze the nonlinear damage responses of continuous fiber toughened composites. Comput Mech 2017;60(3):393–408.
[37] Biro LP, Khanh NQ, Vertesy Z, Horvath ZE, Osvath Z, Koos A, et al. Catalyst traces and other impurities in chemically purified carbon nanotubes grown by CVD. Mater Sci Eng C 2002;19(1–2):9–13.
[38] Kim GM, Nam IW, Yoon HN, Lee HK. Effect of superplasticizer type and siliceous materials on the dispersion of carbon nanotube in cementitious composites. Compos Struct 2018;185:264–72.
[39] Krause B, Mende M, Pötschke P, Petzold G. Dispersability and particle size distribution of CNTs in an aqueous surfactant dispersion as a function of ultrasonic treatment time. Carbon 2010;48(10):2746–54.
[40] Zeng Y, Lu G, Wang H, Du J, Ying Z, Liu C. Positive temperature coefficient thermistors based on carbon nanotube/polymer composites. Sci Rep 2014;4:6684.
[41] Cao J, Chung D. Electric polarization and depolarization in cement-based materials, studied by apparent electrical resistance measurement. Cement Concrete Res 2004;34(3):481–5.
[42] Pan Y, Weng G, Meguid S, Bao W, Zhu Z-H, Hamouda A. Percolation threshold and electrical conductivity of a two-phase composite containing randomly oriented ellipsoidal inclusions. J Appl Phys 2011;110(12):123715.
[43] Qian H, Greenhalgh ES, Shaffer MS, Bismarck A. Carbon nanotube-based hierarchical composites: a review. J Mater Chem 2010;20(23):4751–62.
[44] Park SH, Jang YH, Geem ZW, Lee SH. CityGML-based road information model for route optimization of snow-removal vehicle. ISPRS Int J Geoinf 2019;8(12):588.